Numerical Simulation of Asphalt Compaction and Asphalt Performance*

Pengfei Liu[1], Chonghui Wang[1], Frédéric Otto[1], Jing Hu[2], Milad Moharekpour[1], Dawei Wang[1, 3], Markus Oeser[1]

[1] Institute of Highway Engineering, RWTH Aachen, Germany
[2] School of Transportation, Southeast University, P.R. China
[3] School of Transportation Science and Engineering, Harbin Institute of Technology, P.R. China

Abstract. Asphalt pavement compaction is important, and it can determine the service quality as well as durability of pavement. In recent years, numerical methods have been extensively used to simulate and study the construction process of asphalt pavement and mechanical properties of asphalt mixtures. In the following sections, the compaction process, considering the interaction between the materials and the equipment, is simulated, and the influence of different compaction methods on the mechanical performance of asphalt mixtures is investigated. To achieve this goal, a pre-compaction model is developed using the Discrete Element Method (DEM), and the model of both materials and the paving machine are generated separately. After the pre-compaction simulation, the theory of bounding surface plasticity is combined with the theory of Finite Element Method (FEM) as well as with a kinematic model of a roller drum to simulate the asphalt mixture behavior during a roller pass. In order to ensure consistency both in the laboratory compaction and in-situ compaction, the Aachen compactor has been developed. The effect of different compaction methods (Field, Aachen and Marshall Compactions) on the asphalt specimens is compared and evaluated using the microscale FEM.

Keywords: Numerical Simulation · Asphalt Compaction · Asphalt Performance · Discrete Element Method · Finite Element Method.

1 Introduction

To provide the basis for the future design of durable pavements through a holistic physical analysis of the pavement – tire – vehicle system, the focus of this chapter is on developing a basic understanding of the machine-material interaction behavior during the asphalt compaction process and the mechanical performance of asphalt mixtures. In particular, the processes involved in the in-situ paver and roller compaction of asphalt will be systematically researched by numerical simulations at meso- and macro-scales.

* Funded by the German Research Foundation (DFG) under grant OE 514/1.

Asphalt pavement compaction is one of the most vital phases during road construction, which can determine the service quality as well as the durability of the pavement. During the process of pavement construction, the compaction process consists of two main stages. In the first stage, the compaction is achieved by the paver. It can be called preliminary compaction or paving compaction. In the following stage, the final compaction can be achieved using different combinations of rollers (static, vibrating, pneumatic, etc.) [13]. Therefore, the required density of pavement compaction can be attributed to the initial density compacted by the paver and the final density behind the rollers [58]. According to the construction guidance from different countries, the evaluation on the quality of pavement compaction normally relies on the required density and is always assessed after the final compaction finished by rollers [5]. Xu et al. have proven that adequate preliminary compaction achieved by the paver can guarantee the overall quality of compaction and, furthermore, it can be very helpful for rolling compaction (e.g. reduce the passes of roller compaction) [67].

One of the core parts of a paver that comes into use during the pre-compaction stage is the screed, which works as a vibrating compactor while paving the material using its own weight. Generally, a screed of a paver consists of a tamper and the screed plates, which accommodate the compacting systems to provide high density, smooth surfaces, and durable results [3, 4, 22]. During the pre-compaction, the paving angle is very important; the optimized angle of paving compaction indicates the optimized position of the tamper. Theoretically, the operation of the screed vibration and the paving speed are also determined by the type of material, the mixture gradation, and the paving temperature, as these factors have direct influence on the quality of paving compaction [58, 61].

Although it is possible to achieve a high level of preliminary compaction with the paver (between 75 % and 95 % of Marshall density, depending on the setting of the compaction systems), the remaining compaction increase required in order to achieve the final compaction level (depending on the requirements) is obtained via the use of rollers. Studies have shown that while the compaction systems of the paver subject the material primarily to impact compaction, the combination of pressure and shear stresses under the roller drum allows the aggregate structure to rearrange horizontally, which affects the stiffness and therefore the overall properties of the material [7, 54].

For asphalt compaction, there are several types of rollers. The most commonly used type of roller is the tandem roller with two smooth drums. Alternatively, it is possible to replace one or both drums with rubber tires. While the drums are defined in shape and create a variable stress distribution in the contact area dependent on the diameter of the drum and the material resistance, the rubber tires will partially adjust themselves to the surface of the material depending on the tire pressure and also on the material resistance [38, 40, 48, 49].

Furthermore, smooth drums can either work as static or as dynamic compactors. Static drums use the weight of the roller in order to achieve a compaction effect, while dynamic drums are equipped with one or several unbalance exciters, creating a dynamic movement in the drum according to three different principles: vibration with one circular exciter, vibration with two exciters rotating in opposite directions (thus creating a directed vibration, which can be adjusted), or a rotational oscillation where

two exciters rotate in the same direction but with a phase shift of 180°. The advantage of the use of dynamic drums lies in the superposition of different compaction effects. While static compactors are mainly used to stabilize the material during the first roller passes, the use of dynamic drums allows for the material to overcome the internal friction between the aggregates and therefore achieves a higher compaction effort [2, 12, 23, 48, 49].

In recent years, computational-aided methods, such as the Discrete Element Method (DEM) and Finite Element Method (FEM) have been extensively used to simulate and study the construction process of asphalt pavements and the mechanical properties of asphalt mixtures [1, 25, 35, 62]. DEM has attracted significant interest in the simulation of the mechanical responses of granular materials since it was introduced in the 1970s [14, 15]. This simulation method can provide an innovative and effective approach to enhance the understanding of building materials' properties [9, 36, 43]. In DEM simulation, bulk materials are usually treated as an assembly of two-dimensional (2D) disks or three-dimensional (3D) spheres [14, 15], or else as clumps of these shapes made by rigidly connecting and overlapping multiple disks or spheres [19, 20, 45].

When the material flow inside the paver is described with the use of DEM, the computational effort increases with the number of generated particles [35, 36]. Furthermore, describing the compaction behavior of the asphalt mixture during the roller compaction phase requires the definition of a sufficiently large model in order to take the rolling movement of the drum itself into account. For modeling the macroscopic behavior of the asphalt layer in its preliminary compacted state and during a roller pass, continuum mechanics (i.e. FEM) can be used, as seen in [27].

However, it is necessary to use an adequate constitutive law in order to describe the complex behavior of asphaltic material during the compaction process. In general, the mechanical behavior of asphalt mixtures can be considered as elastic-visco-plastic. The elastic properties are mainly determined by the properties of the single aggregates, the plastic flow by the combined aggregate pile, and the temperature dependent combined visco-elastic and visco-plastic component by the asphalt mortar. In its initially stacked state, the aggregates possess few contact points and are mostly connected by the asphalt mortar. When subjected to external loads, the aggregates begin rearranging, which causes plastic as well as time-dependent visco-plastic deformations, the latter being caused by the deformation resistance exerted by the mortar. While the number of air voids is reduced, the number of contact points between the aggregates increases, thus enabling the material to support higher loads. As a result, plastic deformations will be fewer with every additional load applied while the percentage of elastic deformations with respect to the overall deformation will increase [21, 27, 42]. One possible method to take into account the effects described above is the use of the theory of bounding surface plasticity combined with the theory of the critical state, commonly used in geo-mechanics. Such constitutive laws have already been used in the past to model the plastic behavior of soils as well as asphaltic materials under cyclic loading conditions [24, 28, 30, 51].

After the compaction process, the mechanical properties of the asphalt mixtures should be further investigated by experimental and numerical methods. Asphalt mix-

tures are a typical heterogeneous composite material consisting of aggregates with an irregular shape and random distribution, asphalt binder, and air voids at the microscale. In many microscale simulations, the numerical model explicitly represents the individual components of the heterogeneous internal material structure of asphalt mixture. As a result, specific material models can be assigned to each component in the microscale model. Since the physical effects such as the propagation of microcracks or failure of the interface between aggregates and asphalt mortar are considered separately in microscale simulations, rather simple material formulations can be used for each material phase to represent the complex macroscopic material behavior of asphalt mixture.

In this chapter the compaction process, considering the interaction between the materials and the equipment, is simulated, and the influence of different compaction methods on the mechanical properties of asphalt mixtures is investigated. Before the simulations, important microstructure characteristics (such as morphology of aggregates) are investigated, which have a significant influence on the compaction process and, thus, damage resistance and the durability of asphalt pavements. The details of research strategy and methods can be found in Chapters “Computational methods for analyses of different functional properties of pavements” and “Characterization and evaluation of different asphalt properties using microstructural analysis”. Afterwards, a pre-compaction model was developed in a DEM simulation, and the model of both materials and the paving machine were generated separately. Selecting the parameters of materials was determined via the laboratory tests, while the setting of the paver’s working operations was set based on the real conditions at the field construction site. After the pre-compaction simulation, the theory of bounding surface plasticity was combined with the theory of FEM as well as with a kinematic model of a roller drum, in order to simulate the asphalt mixture behavior during a roller pass and assess the increase in compaction with respect to the roller operation. In order to calibrate the model, laboratory tests were conducted, in which the material behavior was analyzed under compaction temperature conditions as well as under different types of loading (constant loading as well as cyclic loading). In order to ensure consistency both in the laboratory compaction and in field compaction, a new standardized laboratory compaction method has been developed, namely the Aachen compactor. The computer-generated model was developed to explicitly model the different material components of the asphalt mixtures. Compared to the homogeneous model, the heterogeneous model is more consistent with reality and thus yields more reliable results. The related testing methods of the material properties used in the heterogeneous model can be found from the Chapter “Experimental methods for the mechanical characterization of asphalt concrete at different length scales: bitumen, mastic, mortar and asphalt mixture”. The effect of different compaction methods (Field, Aachen and Marshall Compactions) on the asphalt specimens with regard to the internal structure, mechanical response, and fracture behavior is then compared and evaluated using microscale FEM. Some more advanced microscale models are also introduced at the end of this chapter, and such microscale models, which can be coupled to a macro-model, as shown in the Chapters “Multi-physical and multi-scale theoretical-numerical modeling of tire-pavement interaction” and “Numerical simulation of asphalt pavement

responses under rolling tire load by multiscale approach" to allow for multi-scale analysis. The research methodology of this chapter can be seen in Fig. 1.

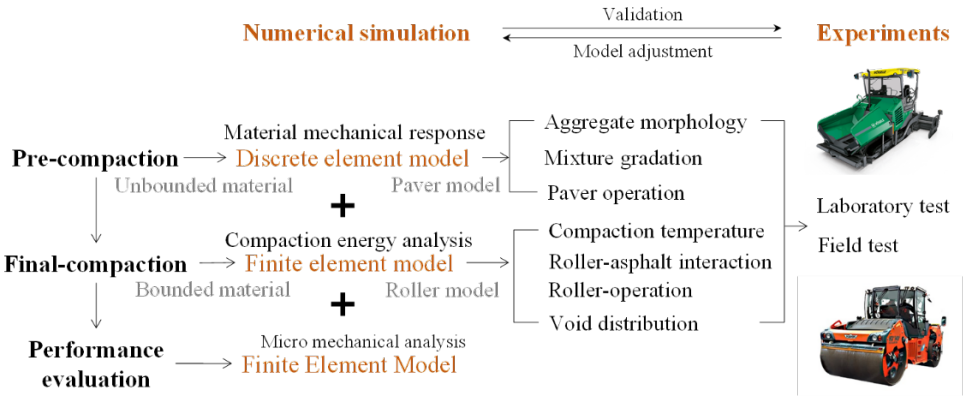

Fig. 1. Research methodology.

2 Simulation of Asphalt Paving Compaction at Mesoscale

The microstructure characteristics of the aggregates are characterized and investigated in this section first. The results can provide basic information for selecting the optimal materials for asphalt compaction. A 3D model based on the DEM was utilized to simulate the pre-compaction of asphalt pavement. The application of DEM in engineering is based on the granular investigations carried out by Cundall and Strack [14, 15]. In DEM simulations, bulk materials are usually treated as an assembly of granular materials interacting at contact points, which can be applied for characterizing the behavior of bulk materials under significant deformation. In the simulation of the pre-compaction of asphalt pavement, the aggregates were generated as clumps with defined morphology consisting of overlapped spherical elements. Newton's second law was used as the basic algorithm to calculate the kinetic behavior of aggregates as well as force-law displacement between the contact points. The equations of motion in the simulation are integrated using an explicit central finite difference algorithm.

2.1 Microstructure Characteristics of Aggregates

The microstructure characteristics of an aggregate (also called morphological characteristics in this section), such as the sphericity, the angularity, and the texture, have a decisive influence on the interlocking, force transmission, and compaction of asphalt mixtures. For this reason, there are strong dependencies between the morphological characteristics of the aggregates and the performance properties of asphalt mixtures. In addition, the morphological characteristics are the most important input values for pavement modeling with numerical methods, e.g., DEM.

The morphological characteristics of 11 types of aggregates were investigated by X-ray Computed Tomography (X-ray CT) in two- and three-dimensions [59, 60, 63, 65]. In order to simulate the polishing process for the road surfacing aggregates, Micro-Deval test (MD) polishing was carried out. The aggregate's morphological properties, such as texture index (TI), 2D Sphericity (2DS), gradient angularity (GA), and 3D angularity (3DA), before and after MD testing were characterized by various parameters calculated from aggregate imaging system (AIMS) and X-ray CT [63]. The Digital Image Processing (DIP) techniques based on X-ray CT images and the detailed description of the four morphological properties are introduced in Chapters "Computational methods for analyses of different functional properties of pavements" and "Characterization and evaluation of different asphalt properties using microstructural analysis".

The GA and 3DA decrease significantly after the MD procedure. The absolute value of change exhibited by the sphericity development is relatively small. The comparison of these four morphological parameters of aggregates before and after MD testing indicated that the AMD state is not dependent on the BMD state. A log-normal function is ideally suited to describe the analyzed morphological characteristics before and after MD. The changes to both the 2DS and the TI only have an ancillary influence [63].

The knowledge obtained from these studies represents an important step regarding the assessment of the polishing resistance of road surfacing aggregate. Furthermore, the morphological properties of the road surfacing aggregate also have a significant influence on the transferable friction between the road surface and the tires, which is analyzed in Chapters "Multi-physical and multi-scale theoretical-numerical modeling of tire-pavement interaction" and "Experimental and simulative methods for the analysis of vehicle-tire-pavement interaction". In addition, the results contribute to the further development of DEM approaches for pre-compaction in this section and also explain the variation of performance characteristics of the roads.

2.2 Development of the Pre-compaction Model in EDEM

There are five steps in the procedure to generate the pre-compaction model in the DEM software EDEM: (1) The geometry sketch of the paver was finished in the computer-aided design (CAD) software AutoCAD, (2) the output from AutoCAD was imported into EDEM as the geometry of paving equipment, the physical properties of the geometries are separately defined with several physical parameters, (3) clumps were generated in EDEM as the templates of particles, the geometrical properties (inertia moment etc.) of the aggregates were calculated via their morphologies, the physical and mechanical properties of them were defined according to laboratory tests, (4) a factory was created in the model for aggregates generation, which was used to define where, when, and how particles appear in the simulation, (5) after defining the parameter that determined the interaction between the paving equipment and bulk material, the aggregates were randomly generated according to the templates, and the size distribution followed the self-defined gradation. Fig. 2 illustrates the model of pre-compaction in EDEM. As seen in the figure, during the simulation,

the paver geometry (auger and paver screed) moves along the negative direction of the x-axis, to compact and pave the material generated. The materials located in the green box are monitored during the pre-compaction process.

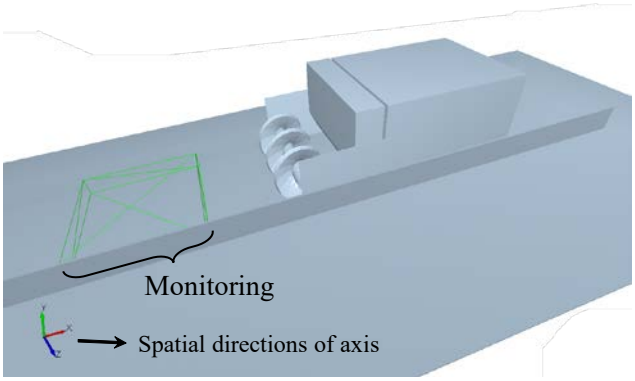

Fig. 2. Pre-compaction model of paver screed in EDEM and its spatial directions of axis.

Some detailed information about the modeling in EDEM will be provided in this section. In the particle simulation, a template was generated first. The shape of the template was simplified as a clump which consisted of three spheres; their relative spatial locations formed the basic shape of a particle model with its sphericity. The basic properties of the template, such as density, Poisson's ratio, and shear modulus were defined in the bulk material feature assembled table. The size distribution is then defined for the particles' generation. The particles are generated randomly from the minimum size to the maximum size of coarse aggregate. Materials can be created directly in the simulation or imported from the materials database.

A factory is created in the model for aggregate generation after the templates have been defined. Particle factories are used to define where, when, and how particles appear in a simulation. Any virtual surface or volume (physical or virtual) can be turned into a particle factory. Factories can only be created if a bulk material has been defined. A simulation can have any number of particle factories. The shape of the geometry which generates particles can be designed by the user; there are also several default geometries such as sphere, box, or facet. There are two types of particle factories which can be used to generate particles: static and dynamic. Static factories produce particles at a specified time. The simulation is paused during particle creation. Dynamic factories produce particles over the duration of a simulation, and the simulation continues as the particles are created.

The mechanical properties of aggregates are determined by a set of mechanical parameters (stiffness and friction between contact points) and geometric characteristics (special assemble, size distribution, and morphology) of particles. As the initial purpose of this study is to model the pre-compaction of asphalt pavement at full-scale, the aggregates are not generated with their real shape due to its requirement for a

prohibitively long calculation period. More capacity of calculation can therefore be imposed for simulating the mechanical behavior of bulk material with large deformation. In future research, the microstructure characteristics of aggregates will be considered in the aggregate generation.

2.3 Contact Model and Parameters

A contact model describes how elements behave when they have contact with each other, which is greatly important in DEM simulation. Therefore, it is explained in detail in this section.

The interaction between bulk material and equipment is defined after the contact model has been generated. The interactions between aggregates can be simplified as a pair of elastic springs with constant normal and shear stiffness properties acting at the contact point. These two springs have specified tensile and shear strengths, which are defined as normal stiffness k_n and shear stiffness k_s. In addition, the frictional behavior is determined by the perfect elastoplastic model via the micro-scaled index friction angle [14]. The elastic contact is imposed on the entire model at macroscopic scale after the local scale contact has been defined, the macro deformation of bulk material then performs based on it. However, this type of contact interaction can only describe the behavior of granular materials without bonding from a binder.

For asphalt materials, one of the significant issues is the bonding with viscoelastic properties. In the DEM simulation, except for the linear contact, another interface between particles is bonded, namely the binder phase, which is modelled by adding a viscoelastic film around each particle. In this model, the thickness of the binder film wrapped on the surface of the aggregates is assumed to be a constant value, which means the binder is assumed to be uniformly attached to the surface of the aggregate. Furthermore, the thickness of the film obtains the correct volume of the binder phase according to the simulated bitumen content. This film can be generated by defining the particle radius and contact radius of a particle, respectively (see Fig. 3).

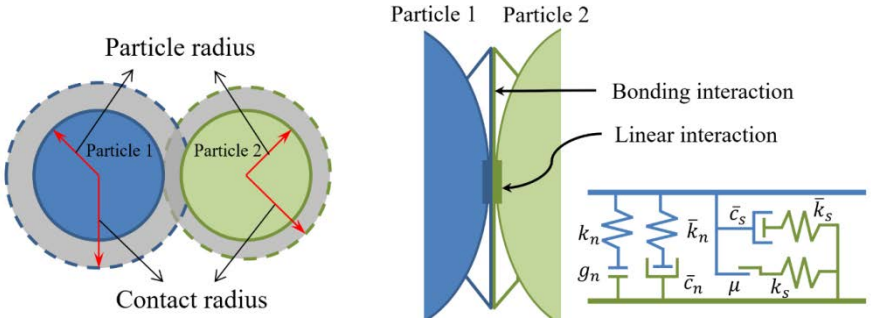

Fig. 3. Visualization of contact between two particles with binder phase.

The viscous bond between two particles acts in parallel with the linear elastic contact. This contact can only be activated when the surface gap of two particles is zero or less

than the sum of the film thicknesses of the two particles. Otherwise, this bond will break and the particles will not stick to each other. Where g_n is the contact gap, k_n and k_s are normal and shear stiffnesses, μ is the friction coefficient, and $\bar{c}_s$ and $\bar{c}_n$ are shear and normal critical-damping ratios. $\bar{k}_n$ and $\bar{k}_s$ are normal and shear stiffnesses of the bond load.

The coefficient of friction and rolling resistance between particle and geometry is defined. The Hertz-Mindlin with Johnson-Kendall-Roberts (JKR) model is selected for particle-to-particle interaction, which can add cohesive behavior to the particles' interaction. The cohesive interaction of this model is defined by the parameter surface energy.

Hertz-Mindlin with JKR cohesion is a cohesion contact model that accounts for the influence of Van der Waals forces within the contact zone and allows the user to model strongly adhesive systems, such as wet materials or asphalt mixtures. In this model, the implementation of normal elastic contact force is based on the JKR theory [53]. Hertz-Mindlin with JKR cohesion uses the same calculations as the Hertz-Mindlin (no slip) contact model for the following types of force: tangential elastic force, normal dissipation force, and tangential dissipation force.

JKR normal force depends on the overlap δ and the interaction parameter, surface energy γ in the following way:

$$F_{JKR} = -4\sqrt{\pi\gamma E^* a^{3/2} + \frac{4E^*}{3R^*}a^3}, \tag{1}$$

$$\delta = \frac{a^2}{R^*} - \sqrt{4\pi\gamma a/E^*}. \tag{2}$$

Here, a is the contact radius, E*is the equivalent Young's modulus and R* is the equivalent radius, which are defined as

$$\frac{1}{E^*} = \frac{(1-v_i^2)}{E_i} + \frac{(1-v_j^2)}{E_j}, \tag{3}$$

$$\frac{1}{R^*} = \frac{1}{R_i} + \frac{1}{R_j}. \tag{4}$$

Here, a is the contact radius, E_i, v_i, R_i, and E_j, v_j, R_j are the Young's modulus, Poisson's ratio and radius of each sphere in contact.

In EDEM, the Hertz-Mindlin mode was applied for calculating the normal and tangential forces, and the JKR here is responsible for the cohesion force calculation. The parameters in the simulation can be seen in Table 1, which were derived from literature studies and laboratory tests, which are introduced in Section 2.5.

Table 1. Material parameters in simulation.

Property	Value	Unit
Young's Modulus	10	GPa
Poisson's ratio	0.25	-
Coefficient of restitution	0.5	-
Coefficient of friction	0.7	-
Density of particles	2500	kg/m^3

2.4 DEM Simulation of the Pre-compaction

In order to study the influence of paver working operations on the quality of pre-compaction during the paving process, different working parameters were selected in this research to simulate the paving process. During the simulation, the paving speed of the paver, the paving thickness of the pavement, and the paving angle of the machine are altered in different models. The paving speed is selected as 5 m/min, 6 m/min, and 7 m/min. The paving angles are chosen as 0°, 1°, and 2°. As for paving thickness, which is the height of pavement after paving, it was chosen as 4 cm, 5 cm, and 6 cm.

During paving compaction in the simulation, different parts of the model geometry have distinct types of movement. The type of geometry can be chosen as physical or virtual, a physical section is an actual surface or volume that particles can interact with. A virtual section (used to create the particle generator) is a surface or volume of interest that does not actually exist and does not interact with anything in a simulation. Sections of paver geometry can be static or dynamic. Static sections remain in a fixed position during the course of a simulation whereas dynamic sections move. Sections can move under translation, rotation, or vibration with a defined frequency. For instance, the test track remains static during the whole process of paving, but other parts such as the paver screed and particles have independent movement depending on the time step.

The tamper and screed plate of the paver both have a vibration in the vertical direction but with different frequencies, which are used for pavement material pre-compaction and surface smoothing. So, the tamper and screed plate are added with "Sinusoidal Translation" kinetic movement, this type of movement can be defined by loop duration, frequency, offset, displacement magnitude, and movement direction. For the auger of the paver, which is used to divide and distribute material evenly on the road surface, this function is achieved by its rotational movement, which is defined by a rotation kinetic option. Besides, all parts of the paver also have a horizontal movement which drags the machine to move forward, which is defined by a stable horizontal velocity.

2.5 Validation of the Simulation Model Based on Experimental Testing

Most of the existing research related to pavement focuses on the final compaction of asphalt mixtures, these approaches cannot produce useful knowledge about changes in arrangement or aggregates interlocking inside materials before the mixture was well compacted. Therefore, a device named Smart Rock (SR) is used in this study, which works based on real-time sensing mechanisms, to provide a scientific basis for enhancing the understanding of asphalt particle rearrangements and flow during the pre-compaction phase. The SR can be used for monitoring the rotation and contact force of an aggregate in real-time. A representative material flow test using SR is introduced in this section, which allows for a closer look at the pre-compaction phase (see Fig. 4).

Different gradations can be considered, in which the aggregates are already evenly mixed with alternated oil. The materials after the mixing test are loosely loaded into a round mold. Before each test, a SR is embedded together with the mixed material, and it is buried under the loading head, at a position slightly to the right of the middle line. And the right edge of the loading head is aligned with the central axis on the SR, which can be seen in Fig. 4. The location of the SR here is selected because during the compacting process, the movement of the SR, especially the rotation is obvious when it is on the eccentric shaft under the loading head. It is no doubt that the well compacted materials have a smaller content of air voids compared to materials in which the compaction degree is not enough, and the compaction process is finished via the rotation and re-arrangement of aggregates during compaction. Therefore, the rotation behavior of aggregates during compaction indicates the re-arranging condition. So, the movement of the SR during compacting can be easily monitored when it is at the location mentioned above. When the compaction test starts, the loading head of the machine keeps moving downward with a constant speed until it goes at a pre-set distance. The measured movement of the SR can be used for validation of the DEM model in a future study.

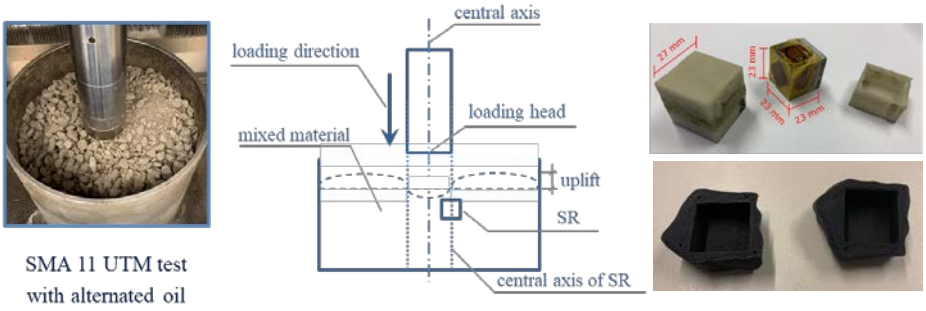

Fig. 4. Material flow test for studying the initial stage of pre-compaction using SR.

Considering variation between simplified or ideal experiments in the laboratory and field tests, the real condition of pavement pre-compaction was accomplished in the test track. The investigation was carried out on the test track of the MOBA Company in Germany. During the paving process, the paver was driven at a speed of around 5 m/min, and the tamper was operated at 30 Hz. First, the bulk materials were loaded into the paver machine. Secondly, sensors were installed on the paver screed to measure the traction during the paving compaction. The following stage was to study the paving behavior via several working parameters of the paver, namely paving velocity, paving thickness, and paving angle. In the end, the paving condition variation in different working operations was compared based on the derived data from sensors. The field test for paver traction monitoring and paving process investigation can be seen in Fig. 5.

In the DEM paving model, the validation was finished by comparing the relationship between the traction of the paver machine and its vertical supported force. The derived data of the paver from the field test was compared to the results generated in

the DEM model with different working parameters. Finally, the model which was closest to real conditions was selected for further study.

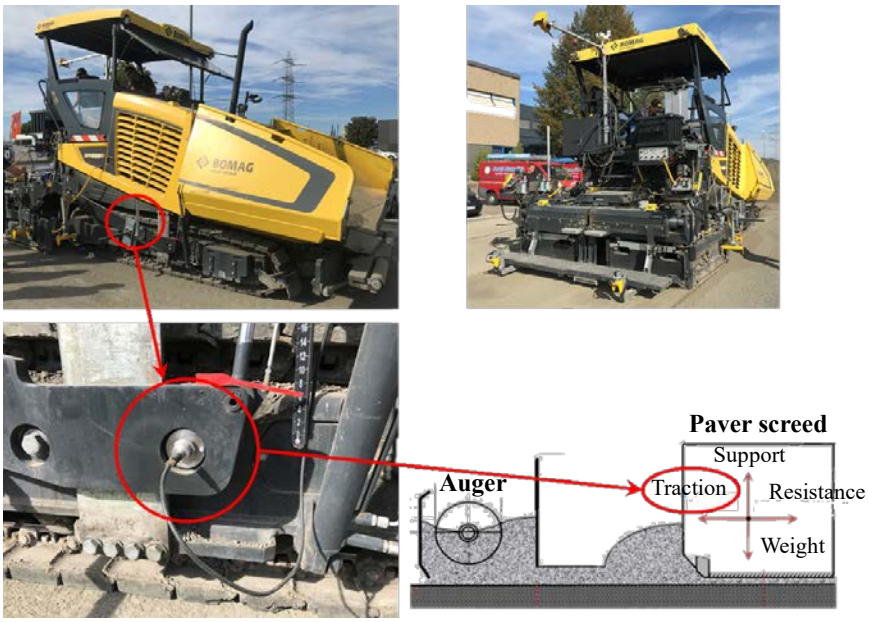

Fig. 5. Traction validation of paver in field test.

The model of pre-compaction uses the real physical parameters of the paver machine and the bulk material in order to simulate the physical conditions of the paving process. The movement of the paver, moving forward with a vertical vibration, was defined by a horizontal velocity per second. Several models with different working parameters were simulated for parameter adjustment and validation. The total amount of the particles with their parameters was kept the same in all of the models, so that the mechanical behavior and the kinetic properties could be compared according to the same conditions. For instance, the contact force between the paver screed and material was analyzed first in this research. As can be seen from Fig. 6, the contact force between the paver and material significantly changes depending on the paving thickness. The blue points indicate the results from simulation, and the orange points indicate the results obtained from field tests.

The relationship between the contact force and the paving thickness yields the distribution function according to mathematical statistics analysis. The vertical contact force, which is also the direction of gravity, dramatically increases as the paving thickness decreases. When the supporting force from materials to the paver equals to the gravity of the paving machine, then the paving thickness with this compressive force distribution corresponds to the real condition of the paver moving on the road surface, at which the horizontal force of the device is close to the real traction offered by the engine. The gravity of the paver has been calculated to 91000 N. From this

diagram, when the generating volume of particles remains constant in all models, the real mass of the paver is close to the result from the model with a paving thickness of 4 cm (see Fig. 6). Therefore, the model with a paving thickness of 4 cm can be used for kinetic and mechanical analysis. The horizontal force of the device can be derived from this image, which is 12253 N.

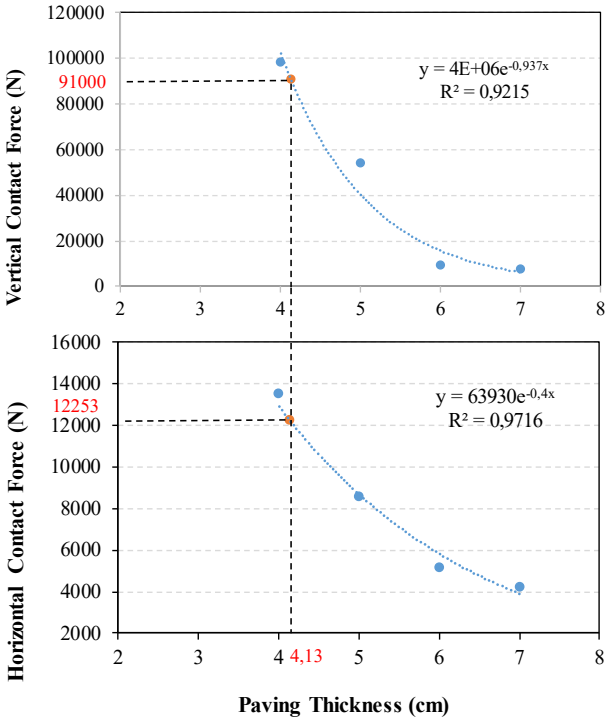

Fig. 6. Test track validation for simulation.

2.6 Influence of Paving Angle on Paving Compaction

The angle of the contacting plane between the material and the paver screed is determined by the special orientation of the paving machine, namely the paving angle of the screed. Therefore, the force distribution can be changed due to the angle of the contacting plane, also because gravity maintains the same directionality. Therefore, the normal stress, shear stress, and friction between the materials and the screed plate are consequently influenced by this angle.

For the DEM simulations, the reference coordinate system and monitoring area can be found in Fig. 2. It is known that the average angular velocities of aggregates have different levels of fluctuation due to the vibration of the paver screed during paving compaction. Furthermore, it is difficult to obtain the overall rotation of aggregates, namely the effective rotation of aggregates. Paving compaction is also a procedure,

during which the aggregates can be pressed and compacted by their relative rotation. The compaction degree therefore can be evaluated by the relative rotational behavior of aggregates. Specifically, the evaluation dominantly considers the rotational properties of aggregates along the driving (z-axis) direction. Fig. 7 illustrates the trend of rotation movement from aggregates during paving. It can be seen from these two figures that the aggregate movement follows a similar trend with same paving speed and thickness, although with different paving angles.

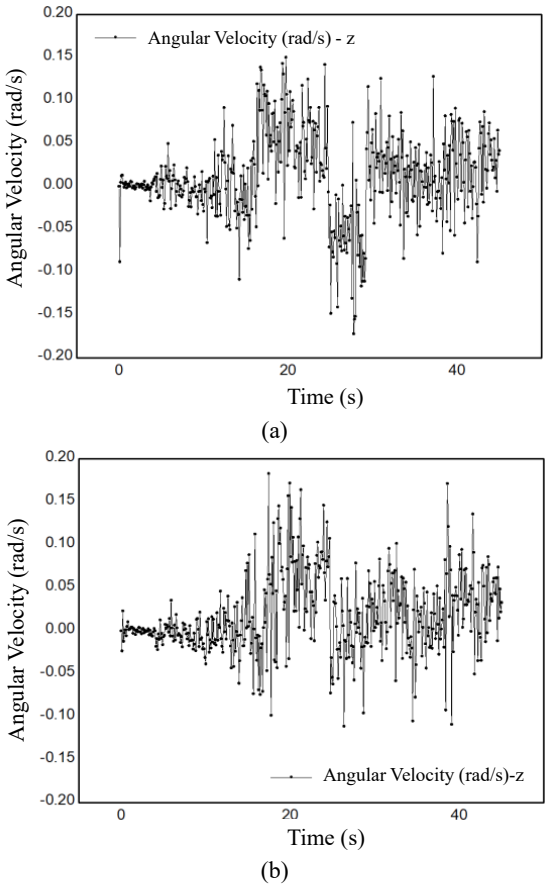

Fig. 7. The trend of average angular velocity around z-axis: paving angle (a) 1°, (b) 2°.

In order to derive the increase in aggregates' effective rotation, this model used a definite integral calculation method. The area enclosed by the curve of angular velocity and the horizontal axis shown in Fig. 7 is calculated and regarded as the average effective rotation of aggregates. In other words, the area calculated for each model is the average effective rotation of aggregates during paving. From the calculated results, the area of 1° paving model is 0.51, and which of 2° paving model is 0.80. It is assumed that the power of the paver screed to the bulk materials remains constant, a

larger paving angle indicates more horizontal components (for the paver moving forward) of paving power are used for rotating the aggregates, and there will be fewer components used for vertical compacting. This result means that a smaller paving angle is better for vertically vibrating compaction.

Fig. 8 shows the comparisons of models with different paving angles; the vertical axis value indicates the final absolute angle of particle rotation, namely the aggregates' effective rotation angle, which was obtained through definite integral calculation. It can be seen from the graph that the effective rotational angle of aggregates performs differently in different rotational directions. However, it should be emphasized that the fluctuation of the rotational angle around both x- and y- directions is not obvious and fluctuated at around 0 rad regardless of the paving angle. On the other hand, the rolling angle following the z-axis changes dramatically when the tamper of the paver starts to contact the particles, fluctuating at a level of more than 0.5 rad. From the results, it can be found that the particles moved obviously around the z-axis, which is parallel to the driving direction, but seldomly move in the other two directions. In other words, during paving compaction, the materials are pre-compacted with a rotation movement of particles around the z-axis; the other two directions do not have obvious rotation. From the results of the simulation, it can also be seen that when the paving angle is 1° or 2°, the increase in compaction density is higher than at an angle of 0°.

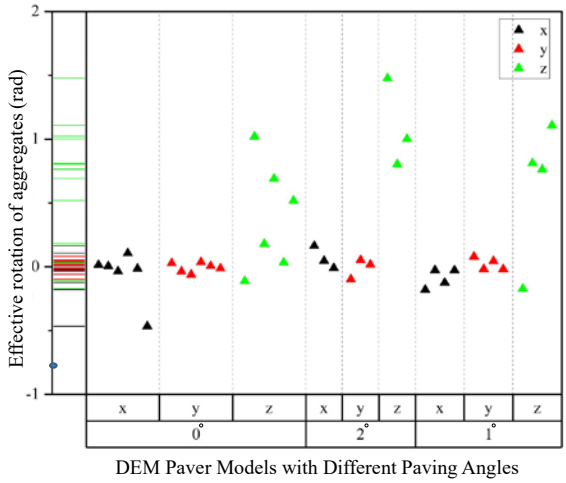

Fig. 8. Effective rotational angle of particles due to different paving angles.

3 Simulation of Asphalt Roller Compaction at Macroscale

After being pre-compacted, it is necessary to use roller compactors in order to reach the requested final compaction level (depending on the requirements formulated in the technical guidelines) of the asphalt mixture layer. Roller compactors apply a combina-

tion of pressure and shear stresses to the asphalt mixture material, which contribute to the increased compaction in the material by rearranging the aggregate structure horizontally [7, 54]. As initially stated, compaction is usually described by the density of the pavement, which increases, while the air-void content of the material decreases.

In this section, the effect of the roller operation on the compaction increase within the asphalt mixture layer is analyzed. For this purpose, a macroscale model of the roller layer interaction is presented, based on previous research [45]. The model needed to fulfill certain requirements, such as representing the movement of the drum (i.e., the rolling movement at different roller speeds as well as the dynamic movement due to different excitations), the contact conditions between the roller and the pavement surface, as well as the behavior of the asphalt mixture when subjected to different types of loading. For this matter, a study on the material behavior under compaction temperatures is presented. This study was conducted through literature analysis and theoretical considerations as well as through laboratory tests, conducted on the material mix. In addition to the reached increase of compaction, an analysis of the void distribution within the layer after the roller pass was conducted as well.

In this section, the pre-compacted asphalt mixture model was described by an FEM model combined with a nonlinear constitutive model (in this case the bounding surface plasticity theory coupled with the critical-state theory), in order to take into account, the material behavior in a loosely stacked state and at compaction temperature conditions. The model is designed in such a way, that the void content in the mineral aggregates (VMA) has a direct impact on the mix properties and therefore the layer properties. Theoretically, the initial conditions of the model (i.e., void distribution before the roller pass) could be defined using the results of the DEM simulations in the previous section. In the underlying study, assumptions regarding the initial state of the layer were made based on practical observations in pavement compaction practice.

Furthermore, the properties of the pavement were determined by laboratory tests. For this purpose, a special laboratory device was designed, which is able to subject the material mix to a variety of triaxial stress states and measure the deformation – including the compression – at compaction temperatures up to 150 °C. The material was subjected to monotonous and cyclic loading in order to capture the effects of time-dependent and repetitive loading. With the help of these tests, the parameters for the constitutive model could be derived and used in order to carry out the simulations of the roller passes at different roller operation modes.

3.1 Basics of Roller Compaction

Usually, several different rollers are used, which differ in their sizes, their total weight, and the type of compaction technology they provide. The number and type of rollers depend on the performance of the paver, the type of asphalt mixtures, and the time window available for compaction. The compact ability of the material is highly temperature-dependent since it is affected by the viscosity of the asphalt binder, which itself increases with the cooling of the asphalt mixture [43]. Therefore, the binder will evolve a higher resistance against deformation and compaction, so that a

higher amount of compaction energy will be required in order to achieve the requested degree of compaction. Studies from [11] have shown an optimum temperature window of 135-155 °C for initiating the roller compaction, outside of which it is still possible to reach the required density with a higher compaction effort, however with a negative effect on the performance properties, such as the indirect tensile strength.

It is, therefore, necessary for the rollers to keep up with the paver, in order to avoid allowing the material to cool off too fast after pre-compaction. The cooling rate itself is dependent on several factors, including meteorological factors as well as the thickness of the layer [11, 26, 64]. Higher pre-compaction values and a lower paving speed can simultaneously decrease the number of required rollers but slow down the construction process. Lower pre-compaction values, on the other hand, require lighter types of rollers for the first roller passes in order to stabilize the material and avoid cracking due to high shear stresses and material displacement. Once the material is stabilized, heavier rollers or rollers equipped with a dynamic drum can be used for breakdown rolling. Furthermore, with lower pre-compaction the number of required roller passes needs to be increased while the roller speed will be reduced in order to achieve a higher increase of compaction with every single pass. Eventually, this will lead to a higher number of required rollers altogether, in order to keep up with the paver [2, 6, 12, 29, 38, 55].

As initially stated, the most common roller type used in pavement compaction is the tandem roller with two smooth steel drums. These drums are defined by the Nijboer number, which is defined as the drum load divided by its width and its diameter. This number should not exceed a certain value, as this could lead to a drum causing more material displacement and cracking instead of compaction. Additionally, the drums can be equipped with unbalance exciters, which create a dynamic movement of the drum (see Fig. 9), allowing for it to overcome the internal friction between the aggregates and therefore achieve a higher compaction effort [2, 12, 23, 48, 49].

As previously stated, the mechanical behavior of asphalt mixtures can be described as a superposition of the properties of its components, which leads to a combined elastic-visco-plastic behavior. The asphalt binder itself manifests combined visco-elastic – thus time-dependent reversible – characteristics at service temperatures, while when reaching the paving and compaction temperature area, the properties can rather be characterized as visco-plastic (time-dependent, irreversible). According to [28], the reversible deformation properties can be neglected at compaction temperatures.

When subjected to an external load, the asphalt mixture will manifest a resistance against deformation, which can be decomposed into initial resistance, internal friction, and the viscosity of the mixture. The initial resistance can be described as an effect resulting from cohesion and interlocking of the aggregates, while internal friction is mainly defined by the current compaction state, the grain size distribution, and the angularity of the aggregates. The viscous resistance of the mixture is defined by the viscosity of the mortar, which is especially active at loose compaction, since the load distribution inside the material happens through the mortar. As the compaction increases, so does the number of contact points, as well as the frictional and initial resistances [27, 42].

It can be derived that the mechanical behavior of asphalt mixtures at compaction temperatures is comparable to the behavior of soils or similar granular materials. Therefore, it is necessary to take certain effects into account, such as the compression and dilation effect, depending on the combination of hydrostatic pressure and shear stresses. These effects, as well as the phenomenon of the stresses tending towards a specific state when the material is continuously sheared, can be described by the use of the critical-state theory [51].

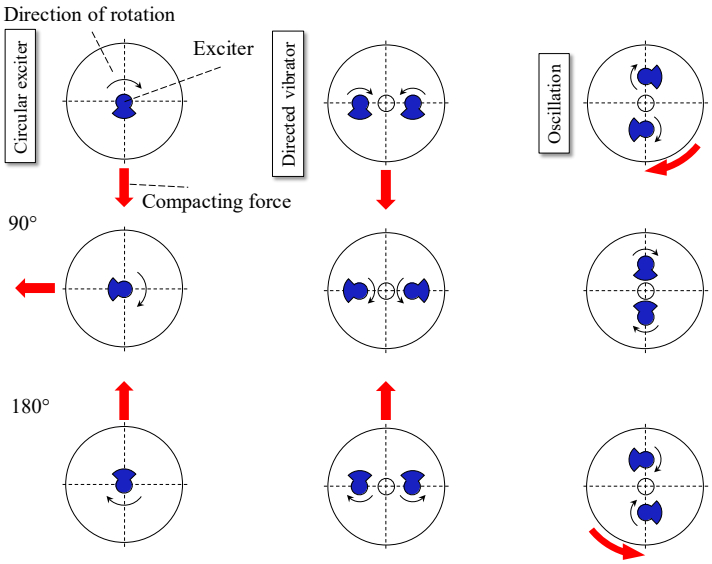

Fig. 9. Principle of different types of dynamic compaction depending on the arrangement of the exciters [49].

3.2 Development of the Roller-asphalt Layer Interaction Model

In this section, the roller compaction is described by using a model, which was developed within the works of [45]. The model consists of three basic parts: a kinematic model of the drum including an excitation unit for oscillation, a contact model (which itself consists of contact conditions for normal contact as well as for dynamic friction between the two contact partners), and the macroscale FEM model of the asphalt mixture layer itself.

All movements are described in a plane coordinate system and on a time-dependent basis. The external loads acting on the system (i.e., the dynamic excitation of the drum) are divided into several time-steps, for each of which, the drum movement response and the corresponding asphalt mixture layer deformation are being computed. This method allows consideration of the continuously changing contact conditions between the drum and the layer due to the translational and rotational drum movement, as well as the oscillatory movement.

The drum itself is assumed as a rigid body and, furthermore, dynamically decoupled from the frame of the roller, as the excitation frequencies of the drum are significantly higher than the natural frequency of the coupled drum-frame system. For each time step, the contact conditions between the drum and the FEM layer model are determined via a radial detection algorithm.

The FEM model is described using a nonlinear constitutive law with plane strain and spatial stress conditions. While conventional plasticity models only take into account plastic deformations when the stress state reaches a defined yield surface, which leads to an abrupt change in the material behavior, the theory of bounding surface plasticity allows a smooth transition to plastic yielding by projecting the stress state onto a defined bounding surface. In this theory, the plastic deformations are calculated with respect to the consistency conditions at the projection point, while at the same time scaling down these plastic deformations dependent on the distance between the projection point and the actual stress state. The definition of an adequate projection rule is one of the key elements in such a model. The theory has been applied in the past for the cyclic loading of unbound granular materials, as well as for asphaltic materials [24, 28, 30, 51]. Furthermore, in [52] the effect of time-dependent behavior due to the temperature-dependent visco-plastic influence of the asphalt binder was considered by implementing consistency based visco-plasticity.

The plastic deformations are calculated, based on the consistency conditions on the bounding surface and the distance of the actual stress point from its projection equivalent. When the actual stress point is identical to the projection center, the deformation is purely elastic. When the stress point reaches the bounding surface, the model behaves similarly to the conventional plasticity theory.

In the underlying study, the theory from [52] combined with the bounding surface formulations from [29] and the stress integration algorithms from [25] were used. In order to differentiate between first-time loading, unloading, and reloading, the projection rules were expanded by additional criteria; Fig. 10 and Fig. 11 demonstrate these rules within the coordinates of the hydrostatic pressure p and the deviatoric equivalent Von-Mises stress q.

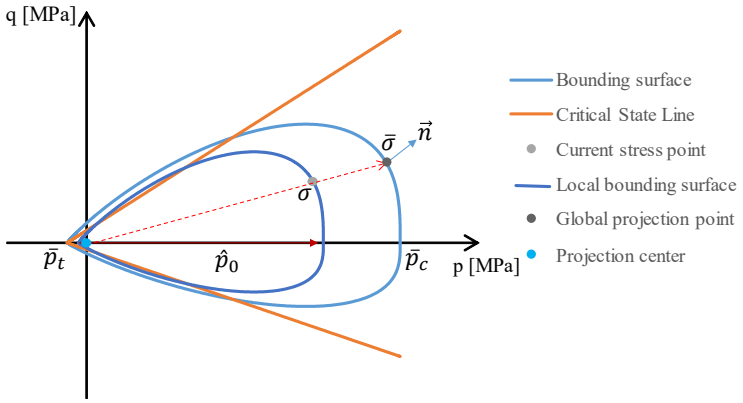

Fig. 10. Projection rules for first time loading [52].

For first time loading, the projection center is located in the origin of the p-q coordinates, from which the projection point $\bar{\sigma}$ is determined via the current stress point σ. From the location of $\bar{\sigma}$ on the bounding surface, a loading surface is derived with the variable $\hat{p}_0$ as a size-parameter, which then is used for determining the hardening parameters. Furthermore, the vector in the normal direction to the bounding surface $\vec{n}$ needs to be determined as well for the calculation of the plastic deformations.

When a stress reversal takes place, the current loading surface will become a local bounding surface, taking into account the previous loading history of the material and the resulting kinematic hardening. The point of stress reversal is now used as a new primary projection center from which a new point $\bar{\sigma}$ and vector $\vec{n}$ on the local bounding surface are determined and forwarded to the global bounding surface via the series of local bounding surfaces, depending on the previous number of stress reversals having taken place. At the same time, the origin of the p-q coordinates remains a secondary projection center, from which a reference point and a reference vector $\vec{n}_{ref}$ will be determined.

For first time loading, both the primary and secondary projection center are identical, which means the respective reference points and the vectors $\vec{n}$ and $\vec{n}_{ref}$ will be identical as well, while for unloading and reloading, $\vec{n}$ and $\vec{n}_{ref}$ will point into different directions. Therefore, the following definition for the different loading states based on the cosine function of the angle between the two vectors were introduced

$$\text{first time loading: } \frac{\vec{n}\cdot\vec{n}_{ref}}{|\vec{n}|\cdot|\vec{n}_{ref}|} = 1, \tag{5}$$

$$\text{unloading: } -1 \leq \frac{\vec{n}\cdot\vec{n}_{ref}}{|\vec{n}|\cdot|\vec{n}_{ref}|} < 0, \tag{6}$$

$$\text{reloading: } 0 \geq \frac{\vec{n}\cdot\vec{n}_{ref}}{|\vec{n}|\cdot|\vec{n}_{ref}|} < 1. \tag{7}$$

With these criteria, the parameters H_f and ξ_f can be computed in a way that takes into account the different loading and unloading paths and control the material stiffness accordingly.

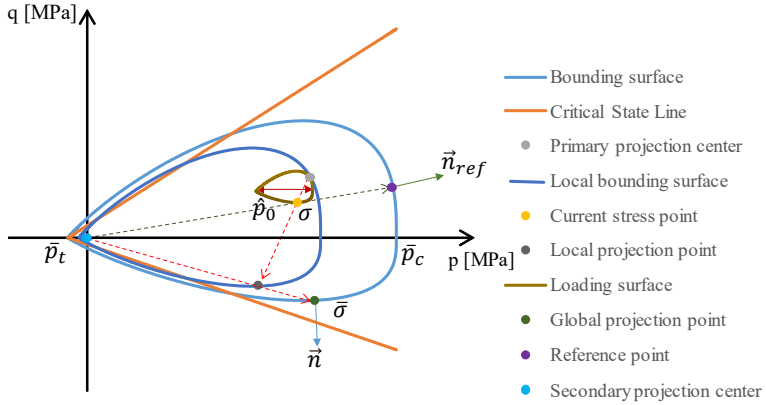

Fig. 11. Projection rules for unloading and reloading [52].

3.3 Calibration of the Developed Material Model

In order to calibrate the material model presented in Section 3.2 and determine the required model parameter, laboratory tests are needed. In [31], triaxle tests were conducted on sand, while in [52] the asphalt mixture models were determined among other tests with uniaxial tensile strength tests. For this study, a special triaxle testing device was developed, in order to be used at compaction temperatures.

The device, as shown in Fig. 12, consists of a metal base-plate in which heating elements were introduced in order keep the material temperature at a constant level during the test. A confinement frame, which is divided into four mobile segments, is mounted on top of that base-plate. Each segment is fixed with the help of a horizontally arranged metal segment, which in turn is equipped with a force transducer, as well as two displacement sensors. The cubic shaped material sample with an initial edge length of 10 cm, is inserted into this confinement frame. The sample can either be prepared in the laboratory (e.g., in a roller segment compactor) or cut from an existing pavement. The initial mass and exact size of the sample need to be determined prior to the test being carried out, so that the initial compaction state is known.

The sample can be pre-heated in an oven and brought up to the required testing temperature within the testing device itself, using the heating elements. Once the pre-heated sample is introduced into the frame, a load can be applied via the top plate. The material deformation and the resulting stress states are determined with the help of the displacement sensors and force transducers. Furthermore, the increase of compaction can be continuously monitored during the test.

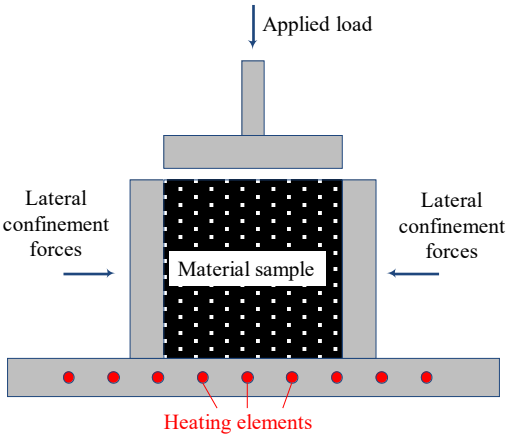

Fig. 12. Schematics of the triaxle testing device used for calibration.

In this study, two different types of testing configurations were carried out at varying degrees of initial compaction. In the first configuration, the vertical load was applied instantaneously and held for a defined time period after which it was released again. This configuration was aimed at determining the time-dependent behavior of the material under constant loading. In the second configuration, the material was subjected

to a cyclic load, in order to analyze the accumulation of plastic deformation as well as the hardening behavior of the material with increasing compaction. The two different testing configurations were carried out using a stone mastic asphalt (SMA) 11 mix, with a polymer-modified asphalt binder. The asphalt binder content was set to 7.0 M.-%. Due to the high number of independent model parameters, assumptions for certain parameters (such as the tensile strength due to cohesion) were made, in order to fit the testing results. The void content VMA at lowest possible stacking was set to 38.7 Vol.-%, which corresponded in the chosen material mix to 75.7 % of bulk density relative to the reference Marshall Density. The tests were carried out at material temperatures between 90 °C and 130 °C in order to determine the temperature-dependent visco-plastic properties.

An example of test results for constant loading can be seen in Fig. 13, where the volumetric strain of the material ϵ_{hyd} is shown as a function of the testing time. The material was subjected to a constant vertical load during the first 30 minutes of the test. During this time span, the material was instantly compressed by 3.1 ‰ during the phase in which the load was built up, followed by another supplemental 2.0 ‰ during constant loading. At t=1800 s, the top load was removed, while the horizontal loads remained active. While parts of the deformations observed at the time point of unloading can be attributed to elastic deformations, switching from a triaxle compressive stress state to a triaxle extensive state will lead to secondary plastic deformations during the unloading phase as well.

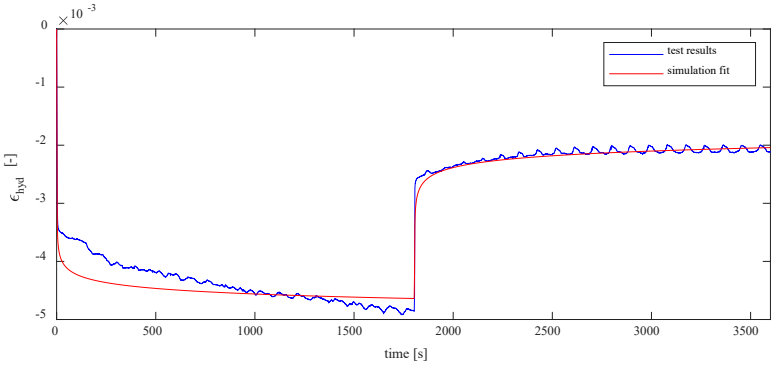

Fig. 13. Test results and parameter fitting of the material model for constant loading.

The effect of cyclic loading was tested in the second testing configuration, of which exemplary test results and the model parameter fitting can be seen in Fig. 14. The material was subjected to a cyclic threshold load with constant amplitude and a frequency of 2 Hz for a duration of 20 minutes. While at the first loading an instantaneous compression of 2.5 ‰ was measured, it can be seen that with each additional loading cycle the cumulated deformation increases, reaching a value of almost 12 ‰ after 20 minutes (corresponding to 2400 loading cycles).

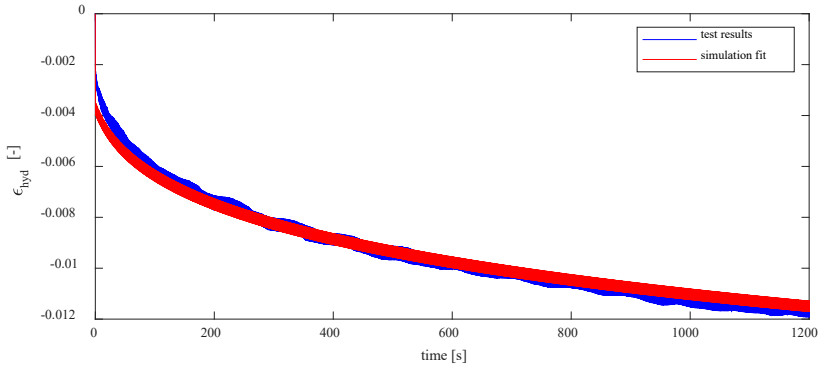

Fig. 14. Test results and parameter fitting of the material model for cyclic loading.

3.4 FEM Simulation of Asphalt Roller Compaction

With the material model presented in Section 3.2 and the material calibration in Section 3.3, roller compaction FEM simulations were run at different roller operation modes in order to study the impact of one roller pass on the increase of compaction and the decrease of the air void content in the resulting asphalt mixture layer. For this purpose, a kinematic model of a smooth steel drum, equipped with a dynamic unit for oscillatory compaction, based on the information from [45], was used in the simulation.

The asphalt mixture layer was defined with a length of 1.5 m in order to allow a sufficiently large enough rolling time at the maximum chosen rolling speed without the roller reaching the end of the layer-model during the simulation. The width of the layer was defined as 1.0 m, which is the exact width of the roller drum itself. The lateral behavior of the material was taken into account via the definition of a spatial stress-state model combined with a plane strain model. The thickness of the layer was chosen as 4 cm, which is a standard value for a typical SMA surface course.

The rigid body model of the oscillatory drum was coupled via the contact model to the FEM-asphalt mixture layer model as described in Section 3.2. The simulation time was set to a total duration of 0.8 seconds, divided into equally sized time-steps with a duration of 0.2 milliseconds, leading to 4000 time-steps. An example of the coupled model can be seen in Fig. 15.

For simplification purposes, the material within the layer model was assumed to be isotropic and fully homogenous in its properties. As such, for every material point in the layer model, the initial content of total voids was set to 26.4 Vol.-%, which corresponds to a density of 90.9 % relative to the Marshall density for the reference mix from the tests in Section 3.3. Also, the material temperature was set to be overall equal to a temperature of 130 °C, so that identical visco-plastic parameters in every material point could be defined, derived from the parameters that were determined at that same temperature in the tests of Section 3.3.

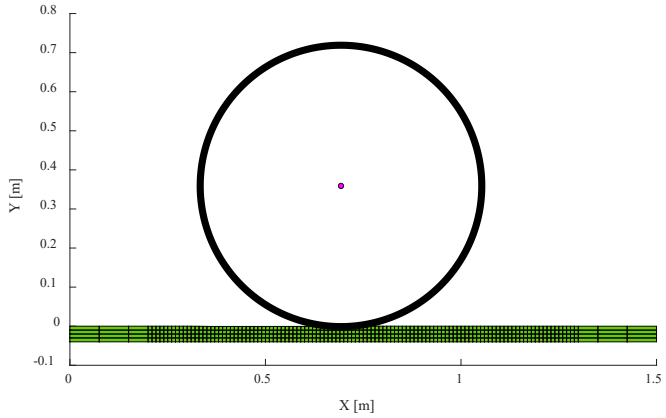

Fig. 15. Roller model with FEM-Asphalt-Mixture-layer.

3.5 Compaction Results and Void Distribution

For roller operation parameters, three different modes (static, oscillating at 27 Hz, and 42 Hz) and two different roller speeds (0.5 m/s and 1.0 m/s) were chosen for this study, leading to a total of 6 simulation runs. For each simulation run, the resulting void distribution within a chosen section of the FEM layer model was determined after one roller pass. As the compaction results in the field are usually determined using a sample (e.g., a core drilled from the layer), this value only represents an average result for the core. As such, with the information of the material mix setup, the resulting average density value relative to Marshall over the layer section was determined. The difference between this value (after one roller pass) and the initial value (before the roller pass) was then calculated and is shown in Table 2 with respect to the different roller operation modes and rolling speeds.

Table 2. Compaction increase after one roller pass at different roller operation modes.

Operation mode	Compaction increase at 0.5 m/s	Compaction increase at 1.0 m/s
Static	+1.6 %	+1.5 %
Oscil. 27 Hz	+2.4 %	+1.8 %
Oscil. 42 Hz	+3.0 %	+2.4 %

The results show that the dynamic movement of the drum contributes to the increase of compaction in this study. Furthermore, it can be seen that high oscillation frequencies and low roller speeds have a stronger effect on the compaction than lower frequencies at high speeds. This effect can be attributed to the number of loading cycles or impacts to which the layer is being subjected during one roller pass, as this number is dependent on the contact time between the roller drum and a single contact point in the layer surface. Higher frequencies and lower rolling speeds will lead to a higher

number of loading cycles, which will lead to a higher compaction, as long as the material stress states remain on the compressive side of the critical state line.

Furthermore, the simulation results allow for determination of the void distribution within the layer. In Fig. 16 the total void (VMA) distribution results after one roller pass at different depths under the layer surface can be seen for a roller speed of 0.5 m/s and a frequency of 27 Hz. The figure shows variations in the void distribution as much in the horizontal direction (X) as in the vertical direction. Reaching almost the bottom of the layer (at -3.5 cm), the total void content is at an average level of 26.4 Vol.-%, which corresponds to the initial value set at the start of the simulation. At levels closer to the surface, a decrease of voids can be observed, up to an average total void content of 22.7 Vol.-% (at a level of -0.5 cm). This can be explained by the fact that the stresses introduced by the roller are highly concentrated in the contact area on the surface and spread over the depth of the layer resulting in overall lower stresses on the bottom of the layer. As a result, the roller possesses a limited depth effect, which results in a stronger compaction effect of the surface zone of the layer.

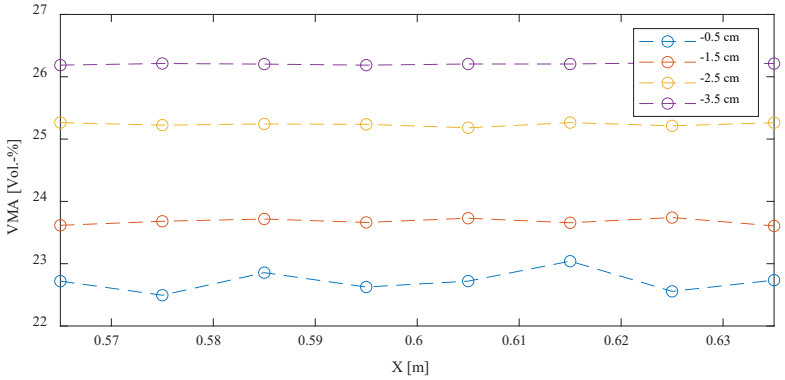

Fig. 16. Total void (VMA) distribution at different levels below the asphalt-mix layer surface (at 27 Hz and 0.5 m/s).

At the same time, it can be seen that the surface area of the layer also shows a higher scattering of values than the bottom area. The results shown in Table 3 indicate that for static roller passes, the scattering of total voids in the horizontal direction of the layer are comparatively low and will produce an even distribution of voids. With the activation of the oscillation, the voids start to show a higher spreading, which increases with the frequency, as well as with the roller speed.

These results indicate that while the dynamic compaction mode leads to a greater increase of compaction with one single roller pass, it also causes more spreading in the void distribution inside the layer. This effect is connected to the multiple different time-dependent stress states to which the different contact points between the roller and the layer surface will be subjected to. For each contact point, the stresses will be dependent on the contact time, the loading frequency, the loading amplitude, and the phase at which the loading starts and will end. Furthermore, these factors are a func-

tion of the size of the contact area between the roller in the rolling direction and the stress distribution within this area. Depending on the constellation of these parameters, the different contact points in the layer surface will be subjected to a different time-dependent constellation of stresses, which in turn will lead to different compaction results, especially on the surface area. The result is an inhomogeneous distribution of voids which can affect the performance properties of the resulting asphalt mixture layer.

Table 3. Scattering of total void contents in the surface area of the simulated layer at different roller operation modes.

Operation mode	VMA scattering at 0.5 m/s [Vol.-%]	VMA scattering at 1.0 m/s [Vol.-%]
Static	± 0.002 %	± 0.002 %
Oscil. 27 Hz	± 0.166 %	± 0.841 %
Oscil. 42 Hz	± 0.399 %	± 0.923 %

It should be pointed out, that this study was only conducted on one single roller pass and with certain simplifying assumptions regarding the distribution of the initial state of material parameters within the layer. For future studies, the effect of several roller passes should be investigated in order to observe the evolution of the void distribution. Furthermore, the initial material parameters within the model should be set with regards to the void and temperature distribution after pre-compaction. For this, the studies carried out with the DEM simulations in the previous section could be used.

4 Simulation of Asphalt Mixtures Manufactured by Different Compaction Methods at Microscale

The mechanical performances of the asphalt mixtures can be influenced by applying the different compaction methods. An innovative standardized laboratory compaction method, named the Aachen compactor, was developed to maintain consistency both in the laboratory and the field compaction [8]. With the Aachen compactor, the cylindrical asphalt samples of two different diameters, namely 100 mm or 150 mm, can be manufactured. (by adjusting the setup, the production of other diameters is technically applicable). As the simulation of the field compaction is the primary aim, the use of two conical rotating steel rollers with a smooth banding, compacting the asphalt mixture in a cylindrical mold achieves the roller compaction principle. Fig. 17 shows the whole compaction procedure with the Aachen Compactor, and this procedure can be generally divided into three stages. Further details can be found in [33].
In this section, the computer-generated approach was used to reconstruct the microstructures of asphalt mixtures with different material components and produced by different compaction methods. Following, the finite element (FE) software ABAQUS was implemented to develop the microstructure-based FE models. The influences of the different compaction methods on the asphalt specimens by using microscale FE

simulation were investigated with comprehensive analyses, which were concerned with the internal structure, mechanical response, fracture behavior etc.

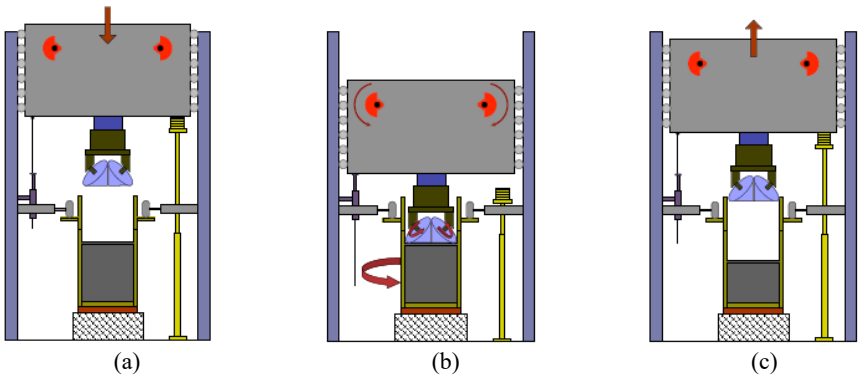

Fig. 17. Operating stages: (a) lowering and pre-rolling stage, (b) main compaction stage, (c) lifting stage [33].

4.1 Preparation of Asphalt Samples and Digital Image Acquisition and Processing

When focusing on a commonly applied asphalt mixture, SMA 11S was used as the samples. In this study, the used binder is Bitumen 50/70. More details about SMA 11S can be found in the Chapter "Experimental methods for the mechanical characterization of asphalt concrete at different length scales: bitumen, mastic, mortar and asphalt mixture". Three different compaction methods were applied to the asphalt samples. 100 mm (diameter) field-compacted cores were drilled from a test track with an approximate 72 mm construction thickness of the paver, which was compacted with a tandem vibration roller.

The Aachen compactor (Aachen specimens) and Marshall compactor (Marshall specimens) were applied to compact the laboratory samples. The field cores' average density was used as a reference for the volume density of the Marshall and Aachen specimens. German guidelines were referred to manufacture the Marshall specimens [16, 17].

Before the surface grinding, storage of all specimens at room temperature lasted for 48 hours. Afterward, they were analyzed with the digital image analysis and numerical simulation. In order to generate the microscale FE model and investigate the internal structure of the asphalt specimens, image analysis was first applied. Before image capturing, the specimens were sawed into two sections, where the horizontal cut proceeded 30 mm below the surface. For each of the three compaction methods, 3 replicates (100 mm diameter) were prepared, for a total of 9 specimens. A high-resolution optical camera was used for all asphalt specimens to capture the cross-section photographs; in order to obtain adequate image quality, the resolution of the images was set to 450 dpi. For further improvement of the image quality, the captured

images were conducted with several procedures in digital image processing (DIP): filter noise, conversion to greyscale images, and binary images to identify objects of interest from the images. To conduct these procedures, the MATLAB Image Processing Toolbox was applied. The selected specimen images are shown in Fig. 18.

Fig. 18. Cross-section images of (a) field cores, (b) Aachen specimens, (c) Marshall specimens [33].

The DIP techniques were applied to derive the long axis distribution of aggregate grains by averaging each replicate samples' parameters. Fig. 19 shows the long axis distribution of aggregate grains for a cross-section. It can be seen that more aggregates with smaller lengths existed the Marshall specimens compared to the other two specimens.

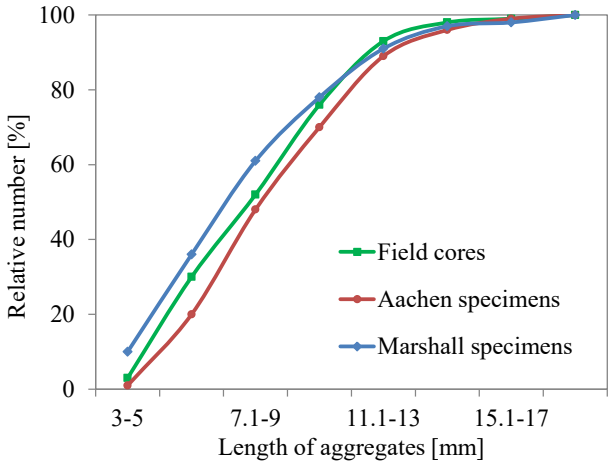

Fig. 19. Relative number of aggregate grains in the cross section (mean value curves) [33].

4.2 Development of Microscale FE Model of Asphalt Mixtures

In order to approach the modeling, the material properties for the aggregate and the asphalt mortar needed to be determined. It is assumed that the asphalt mortar shows linear viscoelastic properties, the results using ABAQUS for a combination of a Prony

series are shown in Table 4. A Young's modulus of 55,000 MPa and a Poisson's ratio of 0.20 was assumed for the linear elastic material behavior of the basalt aggregate [68].

Table 4. Prony series of asphalt mortar at 15 °C.

Item	ρ_m [s]	E_m [MPa]	Item	ρ_m [s]	E_m [MPa]
1	$1.77x10^{-5}$	244.262	7	0.06571	446.172
2	$6.95x10^{-5}$	739.554	8	0.2587	115.784
3	0.0002735	437.066	9	1.0184	119.603
4	0.001077	400.972	10	4.0091	16.708
5	0.004239	487.970	E_∞ [MPa]	3.3521	
6	0.01669	245.953			

The crack propagation may pass through aggregate, asphalt mortar, or the interface layers under consideration of the onset and evolution of damage (i.e., cracking). The material properties of asphalt have a high dependence on temperature. When the temperature is very low, the asphalt mortar is stiffer and some cracks which pass through weak aggregate grains can be seen. As the temperature exceeds 0 °C, very few cracks pass through the aggregate, which leads to more complex failure modes. However, the failure modes are determined by the aggregate morphology, bitumen film thickness, loading rate, and water content [31, 41]. A clear viscoelastic behavior of the asphalt mortar can be observed at 15 °C. This leads to a "self-healing" of micro-cracks or no onset at all because of the relatively low loading speed. Thus, in this investigation, it is assumed that at the interfaces between asphalt mortar and aggregate, the damage and the respective cracks have occurred [42].

Dugdale [19], Barenblatt [10], Rice [48], and others conceived the concept of the cohesive zone model firstly so that crack initiation and propagation could be simulated. According to this concept, resisted by the presence of cohesive forces, fracturing is viewed as a phenomenon where separation occurs between two adjacent virtual surfaces across an extended crack tip (cohesive zone). The implementation of the cohesive fracture behavior in numerical models required the determination of a few parameters. Thus, a static three-point semi-cylinder bending test (3PSCBT) [35] with asphalt specimens complying with the DIN EN 12697-44 [18] was carried out. A high-speed camera (FastCam SA 5) was used during the test to record the specimen. The applied force and the crack tip opening displacement (CTOD) were used for the determination of the required parameters.

The implementation of the adhesive fracture behavior in ABAQUS was considered as linear softening. The constitutive response of the cohesive element was determined by using a bilinear traction-separation law. The initial values for the parameter T° and G_f under consideration of the concept of dissipated fracture energy were determined using the results of the static 3PSCBT [53, 56]. For proper results to fit from the experiment to the numerical simulation, the optimizing of the material parameters was done. They were listed in Table 5.

Table 5. Material parameters for cohesive elements.

Phase	K [MPa]	T° [MPa]	G^f [mJ/mm^2]
Mortar-aggregate interface	14200	3.56	0.344

Fig. 20 shows the 2D models: the aggregates and asphalt mortar are colored in grey and black respectively. For a better illustration of the aggregates and asphalt mortar, the mesh was hidden and due to the small size of the air voids, the air voids are invisible. 4.0 mm was chosen as the minimal grain size of the coarse aggregate and, thus, the asphalt mortar contains the fine aggregate and the coarse aggregates whose size was smaller than 4.0 mm. The cross-section consists of asphalt mortar, air voids, and aggregate with an assumed circularity between 0.7 and 0.8 [40]. To generate the 2D microscale FE models randomly, Neper, an open-source software package for the polygon and polyhedron generation and meshing, was used [47]. A hard contact relation between aggregates as well as in the interface aggregate and asphalt mortar was characterized. Table 5 shows an adhesive failure potential. To discretize the asphalt samples, which contain asphalt mortar and coarse aggregates, linear triangle 3-node plane strain elements (CPE3) were used. For the discretization of the interfaces between aggregate and asphalt mortar, 4-node 2D cohesive elements (COH2D4) were used. After extensive research on mesh, 0.7 mm was selected as the average mesh size of elements in the FE model. 12.7 mm was selected as the width of the loading and support strips for the simulation with the indirect tensile test. Until failure of the specimens, the loading distribution was uniform at a constant deformation rate of 50 mm/min. Horizontal deformation was possible, while the vertical displacement was fixed at the support strip.

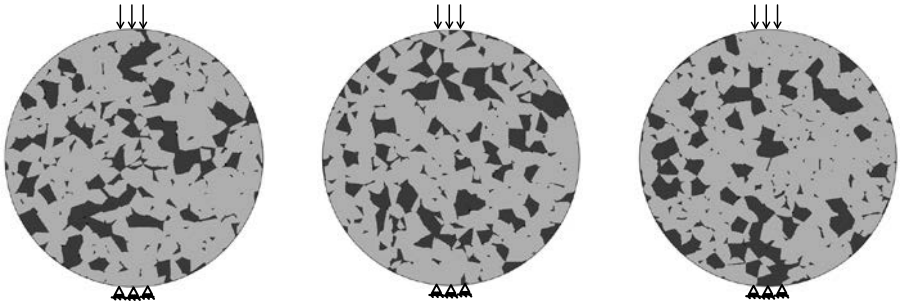

Fig. 20. 2D FE models: (a) Field cores, (b) Aachen specimens, (c) Marshall specimens [33].

4.3 Load-bearing Capacity of the Specimens Manufactured by Different Compaction Methods

The load-bearing capacity of the specimens can be described by the evolution of the applied load and the corresponding displacement of the loading strip. The comparison

of the load-bearing capacities of asphalt specimens, which were manufactured with different compaction methods, was shown in Fig. 21.

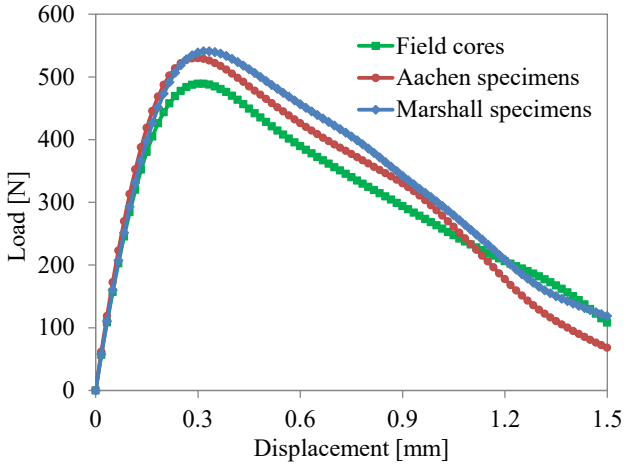

Fig. 21. Comparison of load-displacement curves between models under different compaction methods [33].

All three types of asphalt specimens show similarities in the initial stiffnesses (curves' slope) until the displacement reaches 0.1 mm. As can be seen, the load-bearing capacity of the Marshall specimens is the highest, while the field cores have the lowest value. The Aachen specimens' load-bearing capacity curve is closer to that of the field cores with displacements below 1.0 mm, when compared with the Marshall specimen. During the production process of the Marshall samples, higher compaction energy was applied. Thus, an expectation of a more uniform stress distribution in these specimens, which lead to higher load-bearing capacities, is claimed.

As the slope of the curve strays from its linear path, the micro-cracking begins. When the curve reaches its maximum, the macro-cracking occurs. Once 60 % of the maximum load is reached, complete specimen failure is expected. Table 6 shows the displacements of the loading strip and the corresponding loads. Comparing the values derived from the Aachen specimens and the Marshall specimens, both values of the Aachen specimens fit better to that of the field cores, and this is in accordance with the results observing the curves in Fig. 21.

Table 6. Displacement of the loading strip and the applied loads at different states.

State	Field		Aachen		Marshall	
	Dis. [mm]	Load [N]	Dis. [mm]	Load [N]	Dis. [mm]	Load [N]
Microcrack initiation	0.10	284	0.09	291	0.12	331
Macrocrack initiation	0.31	489	0.30	530	0.33	540
Failure	0.90	294	0.93	318	0.94	325

4.4 Fracture Patterns of Asphalt Specimens

Fig. 22 shows the fracture patterns at the moment of macro-crack initiation in asphalt specimens. Different distributions of the macro-cracking in the asphalt specimens can be observed; in the field specimen, most macro-cracks cumulate in regions of the loading and support strips. However, in the Marshall specimens, this can be found throughout the entirety of the specimens.

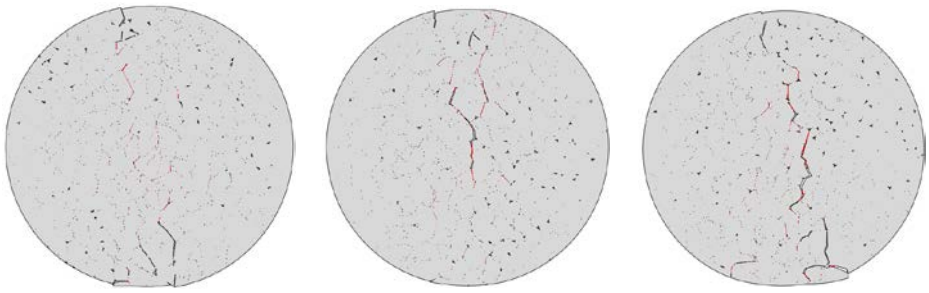

(a) (b) (c)

Fig. 22. Fracture patterns at the moment of macro-crack initiation: (a) Field specimen, (b) Aachen specimen, (c) Marshall specimen [33].

The overall damage of the mortar-aggregate interfaces can be expressed by the damage parameter, i.e., the stiffness degradation. The stiffness of the cohesive elements of the mortar-aggregate interfaces decreases to zero with the increase of the stiffness degradation value from 0 to 1. Therefore, fracturing takes place. The stiffness degradation of the cohesive elements between different compaction methods is analyzed by using the cumulative distribution function (CDF), which is shown in Fig. 23. Exceedance of a limit value is not possible, so all CDFs trail off to the right. Compared to the other two compacted specimens at macro-crack initiation, the ratio of the degraded stiffness in the Marshall specimens is the highest. More cohesive elements are needed due to the damage and fracture for the reduction of the Marshall specimens' stiffness. This is in accordance with the fact that the resistance to permanent deformation increases with the increased stiffness of the Marshall specimens. More similarity in the cumulative distributions of the stiffness can be observed in the field cores and the Aachen specimens. Thus, using the specimens with the production of the Aachen compactor can better predict the crack initiation and propagation in practice than the Marshall specimens.

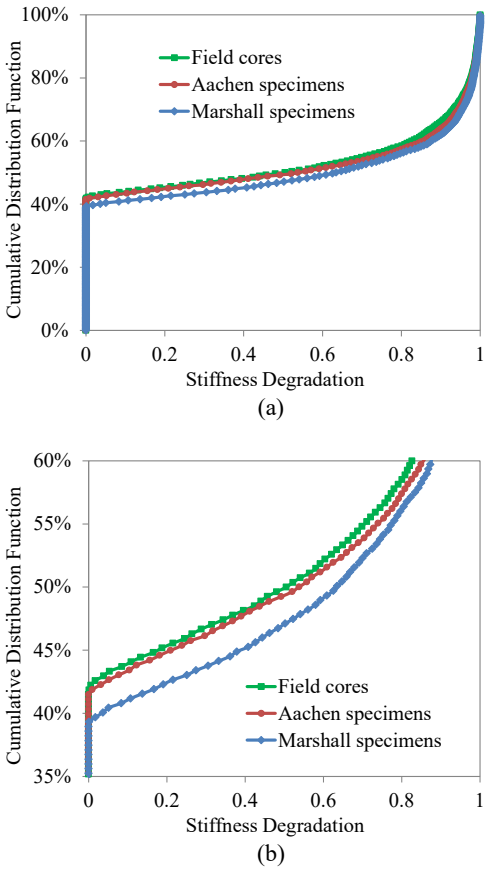

Fig. 23. Cumulative distribution functions of the stiffness degradation for various compaction methods at macro-crack initiation: (a) overall, (b) partial magnification [33].

4.5 Further Development of FE Models of Asphalt Mixtures at Microscale

Besides using the aforementioned FE models of asphalt mixtures to investigate the effect of the different compaction methods on the asphalt specimens, the FE models with different microstructures of asphalt mixtures are further developed in three more studies using both a computer-generation based approach and an image-based approach.

Facing the current global challenges, hydrological cycle recovery and urban flood risk reduction must be taken into consideration. Porous asphalt (PA) is one promising and effective permeable pavement solution, which is characterized by void-rich pavement materials. The performance of PA mixtures can be significantly affected by the fillers used because of the specific gradation. An investigation with the numerical method for the mechanical responses of the PA mixtures influenced by the four dif-

ferent fillers, namely Limestone, Dolomite, Rhyolite, and Granodiorite, was carried out in the first study [38]. The microstructure of PA specimens was detected and reconstructed by using X-ray CT scanning and DIP techniques. An indirect tensile test was simulated by using the 2D FE method to compute and compare the mechanical responses of the PA mixtures (load-bearing capacity, von Mises stress, and creep strain). Based on the results, the mechanical responses of the PA mixtures are considerably affected by the different fillers. A ranking of the performance of the PA mixtures with different fillers was presented. The selection of optimal filler, which improves the permeable pavement design, can be realized based on this ranking.

In the second study, the 3D microscale FE simulations were used to improve understanding of the effect of temperature (-5 °C, 5 °C and 15 °C) on the mechanical performances of the asphalt mixtures [34]. The cross-sectional images of the asphalt specimens were captured by X-ray CT scanning, which were then processed with DIP techniques for the reconstruction of the 3D microstructure of the asphalt specimen. The simulation of the repeat loading triaxial test (RLTT) on this microstructure and the investigation of the evolution of creep strain, the stress states at the asphalt mortar-aggregate interface, and the variation of energy dissipation of asphalt mixtures were presented. The investigation shows that with the increase of the temperature during the RLTT, the magnitude and amplitude of creep strain increase, and the strain growth rate decreases. Additionally, as the temperature increases, the proportion of larger maximum principal stress at the interface between the asphalt mortar and aggregates increases. The proportion of larger maximum principal stress in both coarser and finer aggregates increases when the temperature increases. Moreover, as the temperature increases, the energy dissipations increase. Before the external load is removed, the dissipation of creep energy is increasing gradually. However, a cyclic variation of the dissipation of strain energy can be observed and it recovers to zero after the external load is removed.

The third study was aimed at studying the effect of aggregate morphology (concentrated on aggregate angularity) on the mechanical response and damage behavior of asphalt mixture [35]. A gradually decreasing aggregate angularity was applied for the creation of four microscale FE models. Analysis of the mechanical response and damage behavior of the models was presented. Based on the results, the load-bearing capacity of the asphalt mixture is significantly affected by the aggregate angularity. There is no linearly proportional variation correlation between the load-bearing capacity and the aggregate angularity. At a defined temperature, the creep dissipation energy of the asphalt mixtures can be slight influenced by the different angularities of the aggregates. In general, the creep strain in asphalt mortar reduces with decreases in the aggregate angularity. For the most part, damage becomes visible at the interfaces near sharp corners of the aggregate, with the help of the visualization technique. A connected damage network with complicated crack bridging and branching is built by the extension of damage bands to their surrounding areas. Lower stress concentrations are led from a lower aggregate angularity, less damage and crack initiation at the mortar-aggregate interfaces occur, also the release of damage dissipation energy is reduced. Negative correlations are determined between aggregate angularity and some kinds of dissipation energy, e.g. damage, friction, and creep dissipation energy.

5 Conclusions and Outlook

To simulate the pre-compaction of pavement via paver machine at the mesoscale, a DEM model was developed in this chapter. The model of both materials and the paving machine were generated separately. Selecting the parameters of materials was determined based on the laboratory test results, while the setting of the paver's working operations was selected based on the real conditions at the field construction site. The chosen parameters in this model that can be adjusted for model validation are the paving speed, paving angle of the paver, and the paving thickness of the road surface.

The generated and presented data indicate much variability in vital parameters of the paver and their influence on pre-compaction. During paving compaction, a larger paving angle causes more horizontal components of paving power to be used for rotating the particles, and thus fewer components used for vertical compacting. This result shows that within a proper range of variation, a smaller paving angle has a better effect on vertical vibrating compaction.

The DEM numerical simulation of pavement pre-compaction in this research is based on simplified granular materials, and the validation of the DEM model is based on general field tests with a paver machine. However, the investigation on the paving compaction is closely related to the morphological distribution of granular materials, and also to the interlocking behavior among aggregates during pre-compaction. In addition, specific lab- and field tests are planned to be conducted for further study of the movement of bulk materials in pre-compaction. For the future study of pavement compaction, the real shape information will be accounted for in simulation, and advanced technology for monitoring the movement of particles will be used during the compaction test.

The simulation of asphalt roller compaction at macroscale was carried out with the help of an FE model describing the asphalt mixture layer, coupled to a kinematic model of a steel roller drum, which in turn was equipped with an oscillatory excitation unit. Both models were coupled with the use of nonlinear contact law, taking into consideration dynamic friction processes within the contact area. For the description of the elastic-visco-plastic deformation behavior of the asphalt mixture at compaction temperature level, a material model, based on the bounding surface plasticity theory, was applied and calibrated with the use of a laboratory device, which in turn was designed specifically for testing the mechanical behavior of asphalt mixtures at compaction temperature level.

The information obtained during the laboratory tests was then used to set up the mechanical properties for an asphalt mixture layer model with a defined initial compaction and temperature distribution. This layer was subjected in different simulations to a roller pass, each being set to different roller operation modes and different rolling speeds. The effect of the different operation modes was then analyzed by the resulting increase of compaction and total void distribution within the layer after one roller pass. The results show that dynamic compaction can contribute to the compaction increase, but at the same time will cause strong local variations in the void content distribution within the layer.

The laboratory tests in combination with the theoretical considerations in the literature study have shown that the used material model fulfills the requirements to describe the mechanical behavior of asphalt mixes at compaction temperature level. For a more thorough study on the compaction progress during different roller passes at different compaction modes and their impact on the final result, the initial state of the layer with respect to the initial void and temperature distribution due to the pre-compaction process needs to be considered. For future studies, the effect of several roller passes should be investigated in order to observe the evolution of the void distribution. Furthermore, the initial material parameters within the model should be set with regards to the void and temperature distribution after pre-compaction, which could be derived from the DEM simulations.

A laboratory compaction device, which is called the Aachen compactor, has been developed to attain a higher correspondence between samples compacted in the laboratory and field compaction. Different compaction methods including the field compaction, Aachen compaction, and Marshall compaction are considered in this research. The indirect tensile test was simulated with 2D FE models to investigate the influence of compaction methods with respect to the mechanical response and fracture behavior. Almost all values derived from the Aachen specimens are closer to those from field cores as compared to the Marshall specimens. The different performances of the asphalt specimens manufactured by the various compaction methods may be a result of higher compaction energies in the Marshall compaction. The uniform impact loading of the Marshall hammer and the absence of a kneading effect are most likely the major reason behind the poor correlation to the field cores. Both the compaction energy and kneading effect have an influence on the aggregate orientation and therefore on the related performance.

In future research, more experimental testing should be carried out with regard to different testing types and different testing temperatures to further prove the advantages of the Aachen compactor. More comprehensive analyses using DIP techniques should be performed to consider the characteristics of the air voids. The 3D numerical models should be reconstructed based on the DIP technique and thus deliver more detailed insights into the mechanical responses and deformation properties of the asphalt specimens than the current 2D models.

References

1. Abbas, A., Masad, E., Papagiannakis, T., Harman, T.: Micromechanical modeling of the viscoelastic behavior of asphalt mixtures using the discrete-element method. International Journal of Geomechanics **7**, 131–139 (2007)
2. Adam, D.: Verdichtung im Asphalt- und Erbau. Hamm, A.G.Steyrermühl (2008)
3. Ahmed, T.M., Green, P.L., Khalid, H.A.: Predicting fatigue performance of hot mix asphalt using artificial neural networks. Road Materials and Pavement Design **18**, 141–154 (2017)
4. Angst, C.: Der Einfluß der Verdichtung auf die mechanischen Eigenschaften bituminöser Schichten. Mitteilungen 1385 (1981)

5. Arand, W.: Zur Wirksamkeit von Hochverdichtungsbohlen. Straße Und Autobahn **41**, 14–22 (1990)
6. Arnold, P.: Aachener Verdichter–praxisadäquate Laborverdichtung von Walzasphaltprobekörpern. Mitteilungen des Lehrstuhls und Instituts fuer Strassenwesen, Erd– und Tunnelbau, RWTH Aachen (2009)
7. Axel, F., Ronald, S.: VÖGELE – Operators Guide. Joseph Vögele AG, Ludwigshafen (2016)
8. Axel, F., Ronald, S.: VÖGELE Einbaufibel. Joseph Vögele AG, Ludwigshafen (2012)
9. Bardet, J.P., Huang, Q.: Numerical modeling of micropolar effects in idealized granular materials. Mechanics of granular materials and powder systems **37**, 85–92 (1992)
10. Barenblatt, G.I.: The mathematical theory of equilibrium cracks in brittle fracture. Advances in applied mechanics **7**, 55–129 (1962)
11. Bijleveld, F.: Professionalising the asphalt construction process: aligning information technologies, operators' knowledge and laboratory practices. Ph.D. thesis, University of Twentw (2015)
12. BOMAG GmbH: Grundlagen der Asphaltverdichtung. BOMAG GmbH, Boppard (2009)
13. Commuri, S., Zaman, M.: A novel neural network-based asphalt compaction analyzer. International Journal of Pavement Engineering **9**, 177–188 (2008)
14. Cundall, P.A., Strack, O.D.L.: Discrete numerical model for granualr assemblies. Geotechnique **29**, 47–65 (1979)
15. Cundall, P.A., Strack, O.D.L.: Modeling of microscopic mechanisms in granular material. In: Studies in Applied Mechanics **7**, 137–149 (1983)
16. Deutsches Institut für Normung: DIN 1996-4: 11/1984, Prüfung von Asphalt - Herstellung von Marshall-Probekörpern. Berlin (1984)
17. Deutsches Institut für Normung: DIN EN 12697-30: 2004, 09/2004, Asphalt - Prüfverfahren für Heißasphalt – Teil 30: Probenvorbereitung, Marshall-Verdichtungsgerät. Berlin (2004)
18. Deutsches Institut für Normung: DIN EN 12697-44: Bituminous mixtures - Test method for hot mix asphalt-Part 44: Crack Propagation by Semi-circular Bending Test. Berlin (2014)
19. Dugdale, D.S.: Yielding of steel sheets containing slits. Journal of the Mechanics and Physics of Solids **8**, 100–104 (1960)
20. Favier, J.F., Abbaspour-Fard, M.H., Kremmer, M.: Modeling nonspherical particles using multisphere discrete elements. Journal of Engineering Mechanics **127**, 971–977 (2002)
21. Favier, J.F., Abbaspour-Fard, M.H., Kremmer, M., Raji, A.O.: Shape representation of axi-symmetrical, non-spherical particles in discrete element simulation using multi-element model particles. Engineering Computations (Swansea, Wales) **16**, 467–480 (1999)
22. Figge, H.: Verdichtungs-und belastungsverhalten bituminöser gemische. Ph.D. thesis, RWTH Aachen (1987)
23. Fischer, A., Schug, R.: VÖGELE Booklet on Paving. Joseph Vögele AG, Ludwigshafen (2017)
24. Floss, R., Reuther, A.: Vergleichsuntersuchungen ueber die Wirkung von Vibrierend und Oszillierend Arbeitender Verdichtungswalze. Tiefbau, Ingenieurbau, Strassenbau **33**, 31–4 (1991)
25. Habte, M.A.: Numerical and constitutive modelling of monotonic and cyclic loading in variably saturated soils. Ph.D. Thesis, University of New South Wales (2006)

26. Hu, J., Liu, P., Steinauer, B.: A study on fatigue damage of asphalt mixture under different compaction using 3D-microstructural characteristics. Frontiers of Structural and Civil Engineering **11**, 329–337 (2017)
27. Ter Huerne, H.L.: Compaction of asphalt road pavements: Using finite elements and critical state theory. Ph.D. thesis, University of Twente (2004)
28. Huschek, S.: Zum Verformungsverhalten von Asphaltbeton unter Druck, Ph.D. thesis, ETH Zürich (1983)
29. Kan, M.E., Taiebat, H.A., Khalili, N.: Simplified mapping rule for bounding surface simulation of complex loading paths in granular materials. International Journal of Geomechanics **14**, 239–253 (2014)
30. Kappel, M.: Angewandter Strassenbau: Strassenfertiger im Einsatz. Springer, Berlin (2016)
31. Khalili, N., Habte, M.A., Valliappan, S.: A bounding surface plasticity model for cyclic loading of granular soils. International Journal for Numerical Methods in Engineering **63**, 1939–1960 (2005)
32. Kim, H., Buttlar, W.G.: Discrete fracture modeling of asphalt concrete. International Journal of Solids and Structures **46**, 2593–2604 (2009)
33. Liu, P., Xu, H., Wang, D., Wang, C., Schulze, C., Oeser, M.: Comparison of mechanical responses of asphalt mixtures manufactured by different compaction methods. Construction and Building Materials **162**, 765–780 (2018)
34. Liu, P., Hu, J., Wang, H., Canon Falla, G., Wang, D., Oeser, M.: Influence of temperature on the mechanical response of asphalt mixtures using microstructural analysis and finite-element simulations. Journal of Materials in Civil Engineering **30**, 4018327 (2018)
35. Liu, P., Hu, J., Wang, D., Oeser, M., Alber, S., Ressel, W., Falla, G.C.: Modelling and evaluation of aggregate morphology on asphalt compression behavior. Construction and Building Materials **133**, 196–208 (2017)
36. Liu, Y., Zhou, X., You, Z., Ma, B., Gong, F.: Determining aggregate grain size using discrete-element models of sieve analysis. International Journal of Geomechanics **19**, 04019014 (2019)
37. Liu, Y., You, Z.: Discrete-Element Modeling: Impacts of aggregate sphericity, orientation, and angularity on creep stiffness of idealized asphalt mixtures. Journal of Engineering Mechanics **137**, 294–303 (2011)
38. Lu, G., Wang, C., Liu, P., Pyrek, S., Oeser, M., Leischner, S.: Comparison of mechanical responses of asphalt mixtures under uniform and non-uniform loads using microscale finite element simulation. Materials **12**, 3058 (2019)
39. McLeod, N.W.: Influence of viscosity of asphalt-cements on compaction of paving mixtures in the field and discussion. Highway Research Record **158**, 76–115 (1967)
40. Mgangira, M.B., Anochie-Boateng, J., Komba, J.J.: Quantification of aggregate grain shape characteristics using 3-D laser scanning technology. Southern African Transport Conference (SATC 2013), Pretoria (2013)
41. Milster, R., Emperhoff, W., Graf, K.: Ratschläge für den Einbau von Walzasphalt. Asphalt-Leitfaden **152**, 51 (2004)
42. Mo, L.T.: Damage development in the adhesive zone and mortar of porous asphalt concrete. Ph.D. thesis, Road and Railway Engineering, TU Delft (2010)
43. Nijboer, L.W.: Plasticity as a factor in the design of dense bituminous road carpets. Elsevier, Amsterdam (1948)

44. Olsson, E., Jelagin, D., Partl, M.N.: New discrete element framework for modelling asphalt compaction. Road Materials and Pavement Design **20**, 604–616 (2019)
45. Otto, F.: Dynamisches Interaktionsverhalten zwischen Oszillationsbandagen und Asphaltoberflächen. Ph.D. thesis, RWTH Aachen University (2020)
46. Potyondy, D.O., Cundall, P.A.: A bonded-particle model for rock. International Journal of Rock Mechanics and Mining Sciences **41**, 1329–1364 (2004)
47. Quey, R., Dawson, P.R., Barbe, F.: Large-scale 3D random polycrystals for the finite element method: Generation, meshing and remeshing. Computer Methods in Applied Mechanics and Engineering **200**, 1729–1745 (2011)
48. Rice, J.R.: Mathematical analysis in the mechanics of fracture. Fracture: an advanced treatise **2**, 191–311 (1968)
49. Römer, A.: Oszillationswalzen - Effektiv verdichten ohne Vibrationsbelastung. Tiefbau-/BauPortal, **7**, 17 (2000)
50. Römer, A.: Verdichtungssysteme für die Asphaltverdichtung. Tiefbau/BauPortal, **126**, 23–6 (2003)
51. Schofield, A., Wroth, P.: Critical state soil mechanics. McGraw-Hill, New York (1968)
52. Shahbodagh, B., Habte, M.A., Khoshghalb, A., Khalili, N.: A bounding surface elasto-viscoplastic constitutive model for non-isothermal cyclic analysis of asphaltic materials. International Journal for Numerical and Analytical Methods in Geomechanics **41**, 721–739 (2017)
53. Solutions, D.E.M.: EDEM 2.6 theory reference guide. Edinburgh, United Kingdom (2014)
54. Song, S.H., Wagoner, M.P., Paulino, G.H., Buttlar, W.G.: δ25 Crack opening displacement parameter in cohesive zone models: experiments and simulations in asphalt concrete. Fatigue & Fracture of Engineering Materials & Structures **31**, 850–856 (2008)
55. Tappert, A.: Verdichtung Bituminoeser Schichten-Erfahrungen mit Hochverdichtungsbohlen. Teerbau-Veroeffentlichungen 43–50 (1985)
56. Velske, S., Mentlein, H., Eymann, P.: Strassenbau, Strassenbautechnik. Reguvis Fachmedien, Cologne (2009)
57. Wagnoner, M.P., Buttlar, W., Paulino, G.H.: Disk-shaped compact tension test for asphalt concrete fracture. Experimental mechanics **45**, 270–277 (2005)
58. Wan, Y., Jia, J.: Nonlinear dynamics of asphalt – screed interaction during compaction : Application to improving paving density. Construction and Building Materials **202**, 363–373 (2019)
59. Wang, C., Wang, H., Oeser, M., Mohd Hasan, M.R.: Investigation on the morphological and mineralogical properties of coarse aggregates under VSI crushing operation. International Journal of Pavement Engineering **21**, 1–14 (2020)
60. Wang, D., Wang, H., Bu, Y., Schulze, C., Oeser, M.: Evaluation of aggregate resistance to wear with Micro-Deval test in combination with aggregate imaging techniques. Wear **338–339**, 288–296 (2015)
61. Wang, H., Wang, C., You, Z., Yang, X., Huang, Z.: Characterising the asphalt concrete fracture performance from X-ray CT Imaging and finite element modelling. International Journal of Pavement Engineering **19**, 307–318 (2018)
62. Wang, H., Wang, C., Bu, Y., You, Z., Yang, X., Oeser, M.: Correlate aggregate angularity characteristics to the skid resistance of asphalt pavement based on image analysis technology. Construction and Building Materials **242**, 1–10 (2020)

63. Wang, H., Wang, D., Liu, P., Hu, J., Schulze, C., Oeser, M.: Development of morphological properties of road surfacing aggregates during the polishing process. International Journal of Pavement Engineering **18**, 367–380 (2017)
64. Wang, H., Bu, Y., Wang, D., Oeser, M.: Dreidimensionale Charakterisierung der Kornform und Scharfkantigkeit von Gesteinskörnungen mittels Röntgen-Computertomographie. Bautechnik **90**, 436–43 (2015)
65. Wendebaum, J.: Nutzung der Kerntemperaturvorhersage zur Verdichtung von Asphaltmischgut im Straßenbau. Ph.D. thesis, Universität Fridericiana zu Karlsruhe (2004)
66. Xie, X., Wang, C., Wang, D., Fan, Q., Oeser, M.: Evaluation of polishing behavior of fine aggregates using an accelerated polishing machine with real tires. Journal of Transportation Engineering, Part B: Pavements **145**, 04019015 (2019)
67. Xu, Q., Chang, G.K., Gallivan, V.L., Horan, R.D.: Influences of intelligent compaction uniformity on pavement performances of hot mix asphalt. Construction and Building Materials **30**, 746–752 (2012)
68. You, Z., Adhikari, S., Dai, Q.: Three-dimensional discrete element models for asphalt mixtures. Journal of Engineering Mechanics **134**, 1053–1063 (2008)